Giant and tunable valley degeneracy splitting in MoTe₂

Jingshan Qi (齐景山),[1] Xiao Li (李晓),[2] Qian Niu,[2,3,4,*] and Ji Feng (冯济)[3,4,†]

[1]*School of Physics and Electronic Engineering, Jiangsu Normal University, Xuzhou 221116, People's Republic of China*
[2]*Department of Physics, University of Texas at Austin, Austin, Texas 78712, USA*
[3]*International Center for Quantum Materials, School of Physics, Peking University, Beijing 100871, People's Republic of China*
[4]*Collaborative Innovation Center of Quantum Matter, Beijing 100871, People's Republic of China*

Valleys in monolayer transition-metal dichalcogenides seamlessly connect two basic carriers of quantum information, namely, the electron spin and photon helicity. Lifting the valley degeneracy is an attractive route to achieve further optoelectronic manipulations. However, the magnetic field only creates a very small valley splitting. We propose a strategy to create giant valley splitting by the proximity-induced Zeeman effect. Our first principles calculations of monolayer MoTe₂ on a EuO substrate show that valley splitting over 300 meV can be generated. Interband transition energies become valley dependent, leading to selective spin-photon coupling by optical frequency tuning. The valley splitting is also continuously tunable by rotating the substrate magnetization. The giant and tunable valley splitting adds a different dimension to the exploration of unique optoelectronic devices based on magneto-optical coupling and magnetoelectric coupling.

Introduction. In many kinds of transition-metal dichalcogenide monolayers, a pair of degenerate valleys in the band structure give rise to novel valley-contrasting physics and potential applications. Electrons with a definite spin can be selectively excited by photons with a given helicity through the valleys, thereby furnishing a unique interface between the two elementary carriers of quantum information [1–4]. The valley Hall effect has also been observed recently, enabling electrical detection and manipulation of the photocurrent [5]. Furthermore, the valley electronic states also possess valley-dependent orbital magnetic moments, which, together with the spin magnetic moment, provide the opportunities for magnetic control of the valleys and multiple electronic and optoelectronic functionalities based on magnetic effects.

Lifting the valley degeneracy in monolayer transition-metal dichalcogenides has been achieved under an external magnetic field in a few recent experiments. However, only small valley splitting, 0.1–0.2 meV/T, can be generated [6–9]. The perfect two-dimensional structure of monolayer transition-metal dichalcogenides provides a convenient platform for electronic-structure modification by the proximity effect. In this Rapid Communication, we propose a strategy to create giant valley splitting in monolayer molybdenum ditelluride (MoTe₂) through proximity-induced magnetic interactions. We use first principles calculations to demonstrate that in MoTe₂ on a europium oxide (EuO) substrate, valley splitting greater than 300 meV can be generated by an induced Zeeman field. The proximity coupling makes interband transition energies valley dependent, enabling selective spin-photon coupling by optical frequency tuning, in addition to circular polarization. We also demonstrate that the proposed valley splitting is highly tunable. The giant and tunable valley splitting from the proximity magnetic effect adds a readily accessible dimension to the valley-spin physics, giving rise to

magneto-optical and magnetoelectric couplings, which offers a practical avenue for exploring unique device paradigms.

MoTe₂/EuO heterostructure. The structure of monolayer transition-metal dichalcogenides, MX_2 (M = Mo, W and X = S, Se, and Te), is shown in Fig. 1(a), which mimics a two-dimensional honeycomb lattice, where two lattice sites are respectively occupied by an M atom and a pair of X atoms. Each M is caged by six X atoms, forming a trigonal prism [pink triangles in Fig. 1(a)]. The inequivalent $K_\pm$ are the vertices of the hexagonal Brillouin zone (BZ) [Fig. 1(b)], where the direct band gaps are located. A typical low-energy band structure of free-standing monolayer MX_2 is shown in Fig. 1(c), where a pair of valleys related by time-reversal symmetry are seen to be degenerate.

An energy scale pertinent to the valley-spin physics is now introduced, to quantify spin splitting within a valley, $\Delta_{\mathrm{spin}}^{v/c,\tau} \equiv E_\uparrow^{v/c,\tau} - E_\downarrow^{v/c,\tau}$, arising from spin-orbit coupling (SOC). Here, v and c refer respectively to valence and conduction bands. Valleys, $K_\pm$, are addressed by the index $\tau = \pm 1$. In the presence of time-reversal symmetry, the spin splittings are equal in magnitude but have opposite signs for two valleys. The magnitude of the spin splitting of the valence bands (∼150–500 meV) is typically larger than that of the conduction bands (∼3–60 meV) [10].

The valley degeneracy is also quantified by another energy scale, $\Delta_{\mathrm{val}}^{c/v,\tau} \equiv E_\uparrow^{c/v,\tau} - E_\downarrow^{c/v,-\tau}$, which is identically zero in the presence of time-reversal symmetry. A Zeeman field can break time-reversal symmetry and lift the valley degeneracy [11–14], whereby $\Delta_{\mathrm{val}}^{c/v,\tau} \neq 0$, as exemplified in Fig. 1(d). Since the valley splitting under an external magnetic field only amounts to ∼0.1 meV/T [6–9], it is of importance to develop alternative strategies to achieve a large valley splitting.

A promising approach to lifting valley degeneracy is to employ proximity interactions in a heterostructure composed of monolayer MX_2 and an insulating ferromagnetic substrate. Here, we study a MoTe₂/EuO heterostructure by density functional theory (DFT) calculations [1,15–22]. The computational method is detailed in the Supplemental Material [23]. This
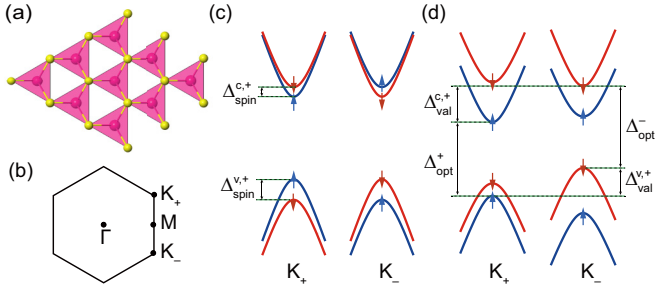
—————
*niu@physics.utexas.edu
†jfeng11@pku.edu.cn

FIG. 1. (Color online) (a) Top view of MX_2 monolayer. Pink/yellow spheres stand for M/X atoms. (b) The Brillouin zone and high symmetry points. (c), (d) Schematic band structure at two valleys of monolayer MX_2 without and with a Zeeman field, respectively. The electronic states with up/down spins are represented by blue/red lines with arrows $\uparrow/\downarrow$.

material selection for the heterostructure is based on two considerations. First, EuO is a ferromagnetic semiconductor with a large band gap of more than 1 eV, and offers an exchange interaction with $\sim 7\mu_B$ spin moment on each Eu ion [24,25]. Second, the lattice mismatch between the MoTe$_2$ and EuO (111) substrate is only 2.7% [23,26,27], a reasonable value for a commensurate heterostructure.

We therefore construct a MoTe$_2$/EuO heterostructure with a slightly strained MoTe$_2$ monolayer placed on the Eu-terminated surface of a EuO (111) substrate composed of 12 Eu/O atomic layers [23], as shown in Fig. 2(a). The oxygen-terminated surface of EuO is saturated by hydrogen, to model a semi-infinite EuO or EuO film grown on another substrate [25,28]. Structural relaxation reveals a few stable configurations for the MoTe$_2$/EuO heterostructure, corresponding to relative shifts of these two materials along the (111) plane of EuO [23]. In the most stable configuration, Mo atoms are located directly on top of the Eu ions, favoring
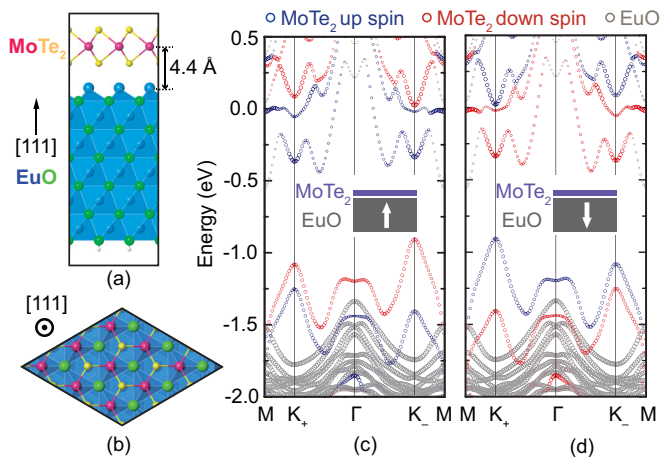

FIG. 2. (Color online) (a) Side view and (b) top view of the heterostructure. (c), (d) Band structures with EuO magnetized upward and downward, respectively. A fat-band representation is used to indicate the projected weights on MoTe$_2$ (blue and red) and EuO (gray). For the MoTe$_2$ projections, blue/red states stand for up/down-spin ones, respectively. The energy scale is zeroed to the Fermi level.

TABLE I. Important energy scales of valley and spin, for a MoTe$_2$ monolayer and a MoTe$_2$/EuO heterostructure.

Valley splitting (meV)	$\Delta_{\mathrm{val}}^{v,+}$	$\Delta_{\mathrm{val}}^{c,+}$	$\Delta_{\mathrm{val}}^{v,-}$	$\Delta_{\mathrm{val}}^{c,-}$
MoTe$_2$[a] (DFT and LEH)	0	0	0	0
MoTe$_2$/EuO (DFT)	-342	-386	-321	-419
MoTe$_2$/EuO (LEH)	-319	-412	-340	-391
Spin splitting (meV)	$\Delta_{\mathrm{spin}}^{v,+}$	$\Delta_{\mathrm{spin}}^{c,+}$	$\Delta_{\mathrm{spin}}^{v,-}$	$\Delta_{\mathrm{spin}}^{c,-}$
MoTe$_2$[a] (DFT and LEH)	214	-27	-214	27
MoTe$_2$/EuO (DFT)	-168	-449	-496	-356
MoTe$_2$/EuO (LEH)	-142	-455	-517	-348

[a]Free-standing MoTe$_2$; the values are identical for DFT and LEH.

proximity-induced magnetic effects [Figs. 2(a) and 2(b)], which will be focused upon in subsequent discussions.

Figures 2(c) and 2(d) show band structures of a MoTe$_2$/EuO heterostructure, with EuO magnetized upward and downward, respectively (see insets). Based on the fat-band representation, a few bands arise primarily from MoTe$_2$ ranging between -1.5 and 0.5 eV, where the EuO substrate has only a minor contribution. Viewing the MoTe$_2$ bands only, there is a well-defined global gap ranging from -0.9 to -0.4 eV. The direct gaps at $K_{\pm}$ (~ 0.6–0.7 eV) indeed correspond to valleys of MoTe$_2$, which are also supported by the optical selectivity and Berry curvature of the Bloch bands, to be presented shortly.

The identification of MoTe$_2$ bands largely free of hybridization with the substrate leads to the key observation that the valley degeneracy of MoTe$_2$ is substantially lifted. The MoTe$_2$ bands near the gap can be classified as spin up and down, as spin moments near $K_{\pm}$ are dominantly out of plane, along the [111] direction of EuO [23]. Therefore, the valley splitting can be quantified by the magnitudes of $\Delta_{\mathrm{val}}^{c/v,\pm}$, which are as large as 321–419 meV (Table I). Moreover, the smallest energies for the band edge vertical optical transition without spin flip in two valleys—two channels of the spin-photon coupling—become unequal, with $\Delta_{\mathrm{opt}}^+ = E_{\uparrow}^{c,+} - E_{\uparrow}^{v,+} = 886$ meV and $\Delta_{\mathrm{opt}}^- = E_{\downarrow}^{c,-} - E_{\downarrow}^{v,-} = 930$ meV [Fig. 2(c)], and $\Delta_{\mathrm{opt}}^- - \Delta_{\mathrm{opt}}^+$ reaches a substantial value of 44 meV, equivalent to the splitting by a 440-T magnetic field.

Proximity-induced interactions. It is evident that proximity-induced interactions lead to a giant valley splitting in MoTe$_2$. A low-energy effective Hamiltonian (LEH) is then constructed to understand such interactions, which reveals the importance of effective Zeeman and Rashba fields induced by the substrate. The LEH is composed of four parts, $H = H_0 + H_{\mathrm{soc}} + H_{\mathrm{ex}} + H_R$, which correspond, respectively, to the orbital interactions, SOC-induced spin splitting [2], proximity-induced exchange, and Rashba interactions,

$$H_0 = v_F(\tau \sigma_x p_x + \sigma_y p_y) + \frac{m}{2}\sigma_z, \quad (1a)$$

$$H_{\mathrm{soc}} = \tau s_z(\lambda_c \sigma_+ + \lambda_v \sigma_-), \quad (1b)$$

$$H_{\mathrm{ex}} = -s_z(B_c \sigma_+ + B_v \sigma_-), \quad (1c)$$

$$H_R = \lambda_R(\tau s_y \sigma_x - s_x \sigma_y). \quad (1d)$$

Here, electronic states $|\psi_c, \uparrow\rangle$, $|\psi_v^{\tau}, \uparrow\rangle$, $|\psi_c, \downarrow\rangle$, and $|\psi_v^{\tau}, \downarrow\rangle$ are used as bases. $|\psi_c\rangle = |d_{z^2}\rangle$ and $|\psi_v^{\tau}\rangle = \frac{1}{\sqrt{2}}(|d_{x^2-y^2}\rangle + i\tau|d_{xy}\rangle)$ are, respectively, the wave functions

of conduction band minima and valence band maxima at K_τ, which are composed of different d orbitals of Mo. The Pauli matrices s_α and σ_α ($\alpha = 0, x, y, z$) refer to real spin and orbital pseudospins, respectively, and $\sigma_\pm \equiv \frac{1}{2}(\sigma_0 \pm \sigma_z)$. $\boldsymbol{p}$ is the electronic momentum and v_F the Fermi velocity. The spin splitting of the conduction and valence bands due to intrinsic SOC is determined by the parameters λ_c and λ_v, respectively. The effective mass m corresponds to the crystal-field splitting between d_{z^2} and $\{d_{xy}, d_{x^2-y^2}\}$ of Mo [1,2]. B_c and B_v are effective Zeeman fields experienced by the conduction and valence bands of MoTe$_2$, arising from the exchange coupling with the magnetic substrate. The low-energy bands of free-standing MX_2 [Fig. 1(c)] can be described by $H_0 + H_{soc}$ [2].

H_{ex} represents the Zeeman field induced by the substrate, and produces a band structure in Fig. 1(d). The valley degeneracy is broken with $\Delta_{val}^{c/v,\tau} = -2B_{c/v}$, which is independent of the valley index τ. This, however, is inconsistent with the DFT results (Table I). To account for the τ dependence of $\Delta_{val}^{c/v,\tau}$ and considering the surface electric field along the (111) direction, we include a Rashba term H_R [29]. The Rashba interaction further hybridizes the valence and conduction bands and mixes the spin components. Although with the Rashba term, spin is no longer a good quantum number, the out-of-plane spin components still dominate in the valley region [23]. Owing to the Rashba term, $\Delta_{val}^{c/v,\tau}$ become valley dependent. Moreover, based on the LEH model, we have $\Delta_{val}^{c,\tau} - \Delta_{val}^{v,-\tau} = 2(B_v - B_c)$. By comparison with the DFT results (Table I), the effective Zeeman fields for the conduction and valence bands are seen to differ by 30–40 meV, justifying the use of two effective Zeeman fields $B_{c/v}$ which reflect different effective Landé g factors for Bloch states.

Matching the model with the DFT band structure of MoTe$_2$/EuO leads to a semiquantitative clarification of the role of proximity-induced interactions. Among all fitted parameters in the LEH [23], the Zeeman fields, $B_c = 206$ meV and $B_v = 170$ meV, are gigantic, which translates to an equivalent magnetic field over 2937 T. For a comparison, the magnetic field produced by the magnetic dipoles of a semi-infinite array of Eu ions is only $\sim$0.007 T [30]. The Rashba parameter $\lambda_R = 72$ meV is also significant. The relevant energy scales from the LEH with as-determined parameters are in decent agreement with DFT results, as also summarized in Table I.

Discussions. The proximity-induced valley splitting proposed here is attractive, as it creates giant differences in various energy scales between the valleys, which will facilitate the access and manipulation of valleys and spins in a MoTe$_2$/EuO heterostructure. Note that prior to accessing the valleys of MoTe$_2$, we need tune the chemical potential into the MoTe$_2$ gap, which may be achieved by electrical gating or chemical doping. In the ensuing discussions, we will assume that the chemical potential is already within the MoTe$_2$ gap.

Owing to the giant valley splitting in Fig. 2(c), we can selectively create valley polarization with equilibrium doping. Hole doping will give simple access to the valleys of MoTe$_2$, whereas electron doping will be interfered by the substrate's bands. We will therefore focus on hole doping. If doping the heterostructure at the K_- valley [Fig. 2(c)], the up-spin holes may produce a transversal current under a longitudinal in-plane electric field [Fig. 3(a)] [31], which arises from the anomalous velocity of Bloch electrons, $\boldsymbol{v}_a \sim \boldsymbol{E} \times \Omega(\boldsymbol{k})$. Here, $\Omega(\boldsymbol{k})$ is
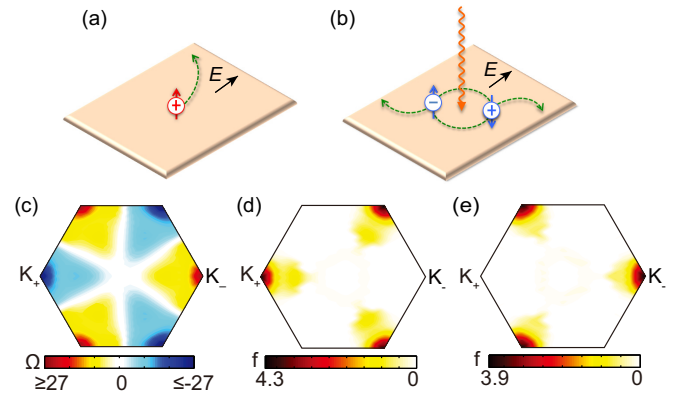

FIG. 3. (Color online) (a), (b) Schematic depictions of the anomalous Hall effects under hole doping and optical pumping, respectively, when EuO is magnetized in the positive [111] direction. Electrons/holes are indicated by circles $-/+$, and the red/blue color follows from band colors in Fig. 2. (c) $\boldsymbol{k}$-resolved non-Abelian Berry curvature (units Å^2) of the valence bands occupied up to the MoTe$_2$ gap of the heterostructure. (d), (e) $\boldsymbol{k}$-resolved optical oscillator strength between the up-spin valence and conduction bands under left- and right-polarized lights, respectively. The counterpart of the down-spin bands is similar and not shown.

the Berry curvature of the Bloch electron [31], and $\boldsymbol{E}$ is the applied electric field. This anomalous Hall effect is the key to the detection of valleys by electric measurements [5,32,33]. It therefore is desirable to have sizable $\Omega(\boldsymbol{k})$, especially near the valleys of MoTe$_2$. In Fig. 3(c), the calculated $\Omega(\boldsymbol{k})$ is sharply peaked in the valley region, with opposite signs for $K_\pm$. Clearly, the valley identity remains intact apart from the giant valley splitting and shall display pronounced anomalous Hall effects. It may be remarked that the flux of the spin holes carries three observable quantities, namely, charge, spin, and valley-dependent orbital magnetic moments, corresponding respectively to anomalous charge, spin, and valley Hall effects [32,33].

The valley identity is also associated with valley-contrasting circular dichroism, which is characterized by the optical oscillator strength under circularly polarized optical fields, $f(\boldsymbol{k})$[23]. As shown in Figs. 3(d) and 3(e), despite the giant valley splitting, the optical absorption of MoTe$_2$/EuO still preserves perfect circular dichroism near the $K_\pm$ valleys. $f(\boldsymbol{k})$ for left-polarized light is sharply peaked near K_+, but is vanishingly small near K_-, and vice versa for right-polarized light, which will allow chiral optical pumping-induced valley polarization in EuO-supported MoTe$_2$, similar to free-standing MoTe$_2$. On the other hand, the proximity coupling makes the interband transition energies valley dependent. This will enable valley selection and corresponding selective spin-photon coupling by optical frequency tuning, with a photon energy $\hbar\omega$ satisfying $\Delta_{opt}^+ < \hbar\omega < \Delta_{opt}^-$, regardless of the light polarization. With $\Delta_{opt}^- - \Delta_{opt}^+ = 44$ meV, the valley selection works over a rather wide spectral range. When a light within this energy range illuminates the sample, only electron-hole pairs from the K_+ valley are generated, leading to a net charge/spin/valley Hall current [see Fig. 3(b)].

The last and very important remark on the proposed valley splitting is concerning its tunability. As EuO has very weak magnetic anisotropy [34], the magnetization direction can be easily rotated by a relatively small magnetic field. As this is a readily accessible experimental knob, it is useful to discuss how the valley splitting depends on substrate magnetization. This can be accomplished with a straightforward generalization of Eq. (1c), $H_{ex} = -\boldsymbol{s} \cdot \hat{\boldsymbol{n}}(B_c\sigma_+ + B_v\sigma_-)$, where $\hat{\boldsymbol{n}}$ is a unit vector denoting the direction of proximity-induced Zeeman fields ($\boldsymbol{B}_{c/v} = \hat{\boldsymbol{n}}B_{c/v}$).

Figures 4(a) and 4(b) show the evolution of the MoTe$_2$ low-energy band structure and valley splittings as functions of the magnetization direction of the EuO substrate, respectively. As the magnetization of the substrate is rotated, the valley splitting changes continuously. When the magnetic field turns from perpendicular to horizontal, the valley splittings for valence bands change by $\sim$46–67 meV, whereas the counterpart for conduction bands $\sim$3–19 meV. The large tunability of valence bands is clearly advantageous, as these bands are unobstructed by states away from the valleys [Fig. 2(c)]. Moreover, with the magnetization reversed from upward to downward, the valley involved in doping and optical excitation will be changed [Figs. 2(d) and 4(a)], and the associated anomalous Hall effects [Figs. 3(a) and 3(b)] become reversed, showing unique magneto-optical coupling and magnetoelectric coupling.

Conclusion. In summary, a general strategy to lift valley degeneracy in a MX_2 monolayer is proposed. As exemplified by computational modeling of a MoTe$_2$/EuO heterostructure, this approach has several advantages. First, the valley splitting is giant, much larger than the band shifts of $\sim$0.1 meV/T by an external magnetic field [6–9]. Second, the giant valley splitting allows for access and manipulation of the valley and spin, both statically and dynamically. Third, the induced valley splitting is highly tunable. The giant and tunable valley splitting adds a readily accessible dimension to the valley-spin physics with rich and interesting experimental consequences, and offers a practical avenue for exploring different device paradigms.
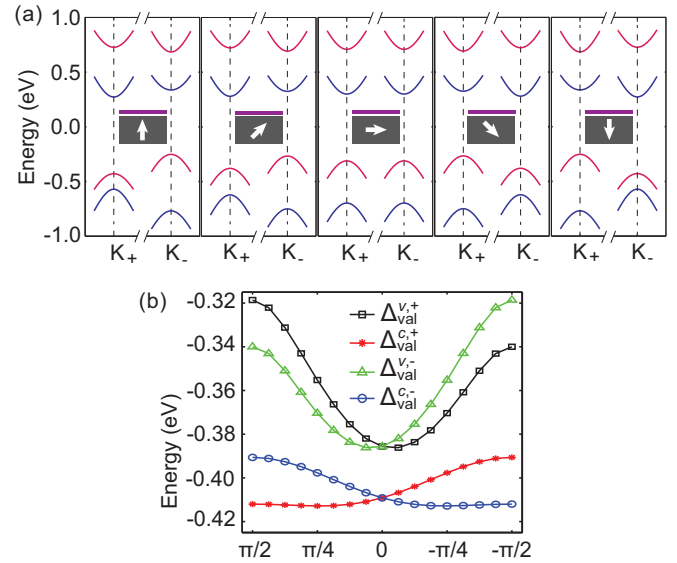

FIG. 4. (Color online) (a) Band structure from the LEH model (momentum range $\pi/5a$ around $K_\pm$, where a is the lattice constant of MoTe$_2$), taking $\hat{\boldsymbol{n}} = (\cos\theta, 0, \sin\theta)$, for $\theta = \pi/2, \pi/4, 0, -\pi/4, -\pi/2$. The spin moment of the blue/red band is parallel/antiparallel to the substrate magnetization. (b) Valley splittings as functions of θ.

[1] T. Cao, G. Wang, W. Han, H. Ye, C. Zhu, J. Shi, Q. Niu, P. Tan, E. Wang, B. Liu, and J. Feng, Nat. Commun. **3**, 887 (2012).

[2] D. Xiao, G.-B. Liu, W. Feng, X. Xu, and W. Yao, Phys. Rev. Lett. **108**, 196802 (2012).

[3] H. Zeng, J. Dai, W. Yao, D. Xiao, and X. Cui, Nat. Nanotechnol. **7**, 490 (2012).

[4] K. F. Mak, K. He, J. Shan, and T. F. Heinz, Nat. Nanotechnol. **7**, 494 (2012).

[5] K. F. Mak, K. L. McGill, J. Park, and P. L. McEuen, Science **344**, 1489 (2014).

[6] Y. Li, J. Ludwig, T. Low, A. Chernikov, X. Cui, G. Arefe, Y. D. Kim, A. M. van der Zande, A. Rigosi, H. M. Hill, S. H. Kim, J. Hone, Z. Li, D. Smirnov, and T. F. Heinz, Phys. Rev. Lett. **113**, 266804 (2014).

[7] D. MacNeill, C. Heikes, K. F. Mak, Z. Anderson, A. Kormányos, V. Zólyomi, J. Park, and D. C. Ralph, Phys. Rev. Lett. **114**, 037401 (2015).

[8] G. Aivazian, Z. Gong, A. M. Jones, R.-L. Chu, J. Yan, D. G. Mandrus, C. Zhang, D. Cobden, W. Yao, and X. Xu, Nat. Phys. **11**, 148 (2015).

[9] A. Srivastava, M. Sidler, A. V. Allain, D. S. Lembke, A. Kis, and A. Imamoglu, Nat. Phys. **11**, 141 (2015).

[10] G.-B. Liu, W.-Y. Shan, Y. Yao, W. Yao, and D. Xiao, Phys. Rev. B **88**, 085433 (2013).

[11] H. Rostami, A. G. Moghaddam, and R. Asgari, Phys. Rev. B **88**, 085440 (2013).

[12] F. Rose, M. O. Goerbig, and F. Piéchon, Phys. Rev. B **88**, 125438 (2013).

[13] T. Cai, S. A. Yang, X. Li, F. Zhang, J. Shi, W. Yao, and Q. Niu, Phys. Rev. B **88**, 115140 (2013).

[14] A. Kormányos, V. Zólyomi, N. D. Drummond, and G. Burkard, Phys. Rev. X **4**, 011034 (2014).

[15] G. Kresse and J. Furthmüller, Phys. Rev. B **54**, 11169 (1996).

[16] S. L. Dudarev, G. A. Botton, S. Y. Savrasov, C. J. Humphreys, and A. P. Sutton, Phys. Rev. B **57**, 1505 (1998).

[17] H. X. Yang, A. Hallal, D. Terrade, X. Waintal, S. Roche, and M. Chshiev, Phys. Rev. Lett. **110**, 046603 (2013).

[18] N. J. C. Ingle and I. S. Elfimov, Phys. Rev. B **77**, 121202 (2008).

[19] P. G. Steeneken, L. H. Tjeng, I. Elfimov, G. A. Sawatzky, G. Ghiringhelli, N. B. Brookes, and D.-J. Huang, Phys. Rev. Lett. **88**, 047201 (2002).

[20] J. S. Moodera, T. S. Santos, and T. Nagahama, J. Phys.: Condens. Matter **19**, 165202 (2007).

[21] X. Li, T. Cao, Q. Niu, J. Shi, and J. Feng, Proc. Natl. Acad. Sci. USA **110**, 3738 (2013).

[22] T. Fukui, Y. Hatsugai, and H. Suzuki, J. Phys. Soc. Jpn. **74**, 1674 (2005).

[23] See Supplemental Material at http://link.aps.org/supplemental/10.1103/PhysRevB.92.121403 for methods, construction of $MoTe_2$/EuO(111) heterostructure, typical configurations and band structures of $MoTe_2$/EuO(111) heterostructure, spin texture of $MoTe_2$-projected bands and parameter fitting of the tight-binding model.

[24] T. R. McGuire and M. W. Shafer, J. Appl. Phys. **35**, 984 (1964).

[25] A. Schmehl, V. Vaithyanathan, A. Herrnberger, S. Thiel, C. Richter, M. Liberati, T. Heeg, M. Rockerath, L. F. Kourkoutis, S. Muhlbauer, P. Boni, D. A. Muller, Y. Barash, J. Schubert, Y. Idzerda, J. Mannhart, and D. G. Schlom, Nat. Mater. **6**, 882 (2007).

[26] R. Sutarto, S. G. Altendorf, B. Coloru, M. Moretti Sala, T. Haupricht, C. F. Chang, Z. Hu, C. Schüßler-Langeheine, N. Hollmann, H. Kierspel, H. H. Hsieh, H.-J. Lin, C. T. Chen, and L. H. Tjeng, Phys. Rev. B **79**, 205318 (2009).

[27] D. H. Keum, S. Cho, J. H. Kim, D.-H. Choe, H.-J. Sung, M. Kan, H. Kang, J.-Y. Hwang, S. W. Kim, H. Yang *et al.*, Nat. Phys. **11**, 482 (2015).

[28] S. Schumacher, D. F. Förster, F. Hu, T. Frauenheim, T. O. Wehling, and T. Michely, Phys. Rev. B **89**, 115410 (2014).

[29] H. Ochoa and R. Roldán, Phys. Rev. B **87**, 245421 (2013).

[30] The magnetic field is computed as the superposition of the magnetic fields produced by the magnetic dipoles of Eu ions (about $7\mu_B$) in a semi-infinite EuO crystal.

[31] D. Xiao, M.-C. Chang, and Q. Niu, Rev. Mod. Phys. **82**, 1959 (2010).

[32] D. Xiao, W. Yao, and Q. Niu, Phys. Rev. Lett. **99**, 236809 (2007).

[33] W. Yao, D. Xiao, and Q. Niu, Phys. Rev. B **77**, 235406 (2008).

[34] N. Miyata and B. E. Argyle, Phys. Rev. **157**, 448 (1967).